JAM CM Journal of Applied Mathematics and Computational Mechanics 2023, 22(3), 5-18
www.amcm.pcz.pl p-ISSN 2299-9965
DOI: 10.17512/jamcm.2023.3.01 e-ISSN 2353-0588

SORET AND DUFOUR EFFECTS ON MHD FLOW OF A MICROPOLAR FLUID PAST OVER A VERTICAL RIGA PLATE

Keshab Borah[1], Jadav Konch[2] , Shyamanta Chakraborty[3]

[1] Department of Mathematics, Gauhati University, Guwahati, Assam, India
[2] Department of Mathematics, Dhemaji College, Dhemaji, Assam, India
[3] UGC-HRDC, Gauhati University, Guwahati, Assam, India
keshabborah388@gmail.com, jadavkonch@gmail.com, schakrabortyhrdc@gauhati.ac.in

Received: 12 April 2023; Accepted: 15 September 2023

Abstract. The present study investigates heat and mass transport phenomena associated with the MHD flow of micropolar fluid over a vertically stretched Riga plate under the action of a uniform magnetic field applied parallel to the plate. The objective of the study is to analyze Soret and Dufour effects on this physical situation in the presence of chemical reaction. The governing partial differential equations are converted into ordinary differential equations using suitable similarity transformations. The equations are solved numerically by developing programming codes in MATLAB for the very efficient shooting method along with the fourth order Runge-Kutta scheme. The velocity, microrotation, temperature and species concentration distribution are presented graphically for various emerging physical parameters like Hartmann number, material parameter, Soret number, Dufour number and other dimensionless parameters. It is found that the species concentration distribution profiles increase with increasing Soret number, whereas the temperature distribution profile decreases with an increasing Soret number. This work also provides solutions for shear stress at plates, the rate of heat and mass transfer in addition to those for velocity, microrotation, temperature and species concentration. Comparisons with previous studies are carefully examined, and it is found that they are generally in agreement.

MSC 2010: *35Q35, 76A05, 76D10*
Keywords: *chemical reaction, Dufour number, micropolar fluid, Riga plate, Soret number*

1. Introduction

The study of the heat and mass transfer flow of micropolar fluids over a Riga plate attracts attention among researchers due to numerous applications in manufacturing and industries. Micropolar fluids are fluids with rotating microcomponents that change the hydrodynamics of motion. This is how a micropolar liquid behaves differently than a Newtonian fluid. Eringen [1, 2] had presented the basic

hypothesis about micropolar fluid and developed the basic and fundamental law. Using this idea, many researchers have developed mathematical models of various non-Newtonian fluids for which the classical Navier Stoke theory does not seem to fit. The mathematical solution for heat transfer in micropolar fluid through an extensible plate was examined by Hassanien and Gorla [3].

Gailitis and Lielausis [4] conducted the initial research on a Riga plate. According to Ahmad et al. [5], a Riga plate generates crossing electric and magnetic fields capable of producing wall parallel Lorentz force, allowing fluid flow to be regulated. Slip dynamics were used by Ayub et al. [6] to control EMHD nanofluid flow over a horizontal Riga plate. The critical importance of a Riga plate is the reduction of viscous and pressure drag on submarines, as well as the prevention of boundary layer separation, according to Hayat et al. [7]. Iqbal et al. [8] discussed the melting heat transport of nanofluidic problem over a Riga plate with erratic thickness using the Keller Box scheme. Rasool and Zhang [9] investigated the motion of a reactive Eyring-Powell nanoliquid over an electromagnetic actuator in a non-porous medium, whereas Fatunmbi and Adeosun [10] focused on the nonlinear radiative flux with heat-mass transfer characteristics and exponential changing viscosity. Reddy and Krishna [11] discussed the effects of Soret and Dufour on MHD micropolar fluid flow over a linearly stretching sheet through a non-darcy porous medium. Reddy et al. [12] studied the effect of the porosity parameter on two-dimensional unsteady magnetohydrodynamic mixed convection heat and mass transport at the stagnation point, taking into account the influence of radiation and viscous dissipation. Goud et al. [13] numerically investigated the effects of Soret, Dufour and chemical reaction on the MHD flow of Casson fluid through an exponentially permeable stretching surface. Mishra et al. [14] investigated the Williamson MHD nanofluid flow through a wedge in porous media with variable viscosity. Goud et al. [15] studied the impact of chemical reaction and Soret effect on an unsteady MHD heat and mass transfer fluid flow over an infinite vertical plate in the presence of radiation and heat absorption. Reddy et al. [16] investigated the numerical solution of steady MHD flow over a stretching horizontal cylinder considering heat source/sink. Goud et al. [17] conducted an analysis of the characteristics of radiation and chemical reaction on the dissipative flow through a porous vertical infinite plate with magnetic and Soret effects. Kumar et al. [18] investigated the impact of non-Newtonian MHD Casson fluid flow along a vertical porous plate, taking into consideration the effects of Soret, Dufour and chemical reaction. Reddy et al. [19] explored the multiple slip effects on steady MHD fluid flow past a non-isothermal stretching surface. Ahmed et al. [20] investigated the Soret and Dufour characteristics of the third-grade fluid due to the stretched cylinder. Recently, a numerical case study of chemical reaction impact on MHD micropolar fluid flow passing over a vertical Riga plate was studied by Goud et al. [21].

To the best of our knowledge, there are no previous studies on micropolar fluid flows generated by expanding Riga plate to investigate the effects of Soret and Dufour in presence of the magnetic field. The following are the novelties of the present study:

- It involves an efficient numerical method with a reasonably good error tolerance for wide range of parameters values. Besides the numerical procedure, the thermo-fluidics considered here have ample applications, where in the configurations may exist as a single independent unit or may be a part of some larger setup.
- Goud et al. [21] neglected the combined impact of Soret and Dufour on MHD micropolar fluid with chemical reaction over a stretching Riga plate, which affects the heat and mass transfer phenomena significantly.

Motivated by the above works, the objectives of this study is to investigate the Soret and Dufour effects on MHD micropolar fluid flow passing over a vertical Riga plate with chemical reaction. This is an addition of Soret and Dufour effects to the problem discussed by Goud et al. [21]. The governing equations of the flow system are solved numerically by developing programming codes in MATLAB for the shooting method along with a fourth order Runge-Kutta initial value scheme. Direct comparison with published results for specific scenarios confirmed the veracity of our present study.

2. Mathematical formulation

We consider a fully developed steady 2-dimensional MHD flow of a micropolar fluid with mass and heat transfer over a Riga plate. The viscous flow caused due to the movement of the Riga plate positioned in an electrically conducting incompressible liquid. It is considered that the x-axis is along the Riga plate.

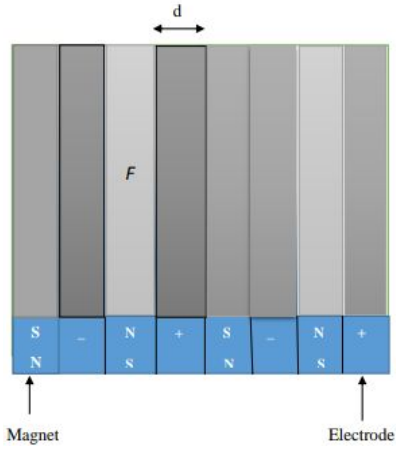

Fig. 1. Geometry of Riga plate

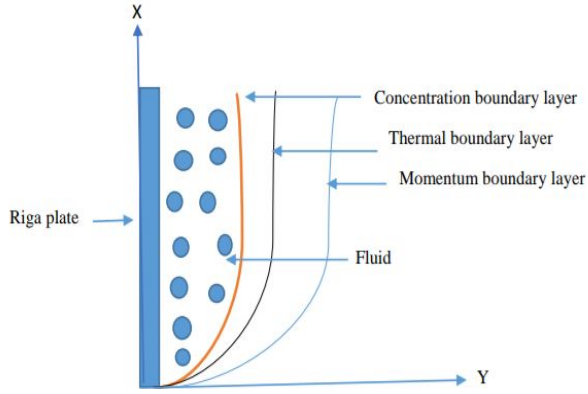

Fig. 2. Physical description of flow system

A uniform magnetic field is applied parallel to the plate along a positive direction of x. The magnetic Reynolds numbers are assumed to be extremely low, and the magnetic force is used along a path perpendicular to a stretched platter and is induced magnetic force. It is assumed that the captivated electrical field is zero

so that the Hall current is negligibly small, and the fluid properties are isotropic and consistent along their length and breadth of the motion. The physical geometry of the plate and the flow are shown in Figures 1 and 2.

With the above assumptions and physical situation, the governing equations in the Cartesian coordinate system are as follows [21]:

$$\frac{\partial u}{\partial x}+\frac{\partial v}{\partial y}=0 \tag{1}$$

$$u\frac{\partial u}{\partial x}+v\frac{\partial u}{\partial y}=\left(\frac{\mu+\kappa}{\rho}\right)\frac{\partial^2 u}{\partial y^2}+\frac{\kappa}{\rho}\frac{\partial N}{\partial y}+\frac{\pi j_0 M_0}{8\rho}Exp\left(-\frac{y\pi}{d}\right) \tag{2}$$

$$u\frac{\partial N}{\partial x}+v\frac{\partial N}{\partial y}=\frac{\gamma}{\rho j}\frac{\partial^2 N}{\partial y^2}-\frac{\kappa}{\rho j}\left(2N+\frac{\partial u}{\partial y}\right) \tag{3}$$

$$u\frac{\partial T}{\partial x}+v\frac{\partial T}{\partial y}=\frac{k}{\rho C_P}\frac{\partial^2 T}{\partial y^2}+\left(\frac{\mu+\kappa}{\rho C_P}\right)\left(\frac{\partial u}{\partial y}\right)^2+\left(\frac{D_M K_T}{C_S C_P}\right)\frac{\partial^2 C}{\partial y^2} \tag{4}$$

$$u\frac{\partial C}{\partial x}+v\frac{\partial C}{\partial y}=D_M\frac{\partial^2 C}{\partial y^2}-k_0\left(C-C_\infty\right)+\left(\frac{D_M K_T}{T_M}\right)\frac{\partial^2 T}{\partial y^2} \tag{5}$$

The boundary conditions of the physical situation are:

$$\left.\begin{aligned} &u=u_w=bx;\ v=0;\ N=0;\ T=T_w;\ C=C_w \text{ at } y=0\\ &u=0;\ N=0;\ T=T_\infty;\ C=C_\infty \text{ as } y\to\infty \end{aligned}\right\} \tag{6}$$

Here, $j=\frac{\upsilon x}{u_w}=\frac{\upsilon}{b}$ is the micro-inertia density that specify the length of the reference, k is the thermal conductivity, N is the microrotation or angular velocity, γ is the spin-gradient viscosity and is given by $\gamma=\left(\mu+\frac{\kappa}{2}\right)j$.

We introduce the following usual similarity transformations:

$$\eta=\sqrt{\frac{b}{\upsilon}}y,\ f\left(\eta\right)=\frac{\psi}{x\sqrt{b\upsilon}},\ g(\eta)=\sqrt{\frac{\upsilon}{b}}\frac{N}{bx},\ \theta\left(\eta\right)=\frac{T-T_\infty}{T_w-T_\infty},\ \phi\left(\eta\right)=\frac{C-C_\infty}{C_w-C_\infty} \tag{7}$$

Using the relation $u=\frac{\partial\psi}{\partial y}$ and $v=-\frac{\partial\psi}{\partial x}$ (where ψ is the stream function), we get $u=xbf'(\eta)$ and $v=-\sqrt{b\upsilon}f\left(\eta\right)$.

Using above substitutions, equation (1) is identically satisfied and equations (2)-(5) are transformed into the following:

$$(1+K)f'''+ff''+Kg'+Me^{-\beta\eta}-(f')^2=0 \tag{8}$$

$$\left(1+\frac{K}{2}\right)g''+fg'-f'g-K(2g+f'')=0 \tag{9}$$

$$\theta''+Prf\theta'+(1+K)PrEc(f'')^2+PrDu\,\phi''=0 \tag{10}$$

$$\phi''+Sc\,f\phi'-ScKc\,\phi+Sc\,Sr\,\theta''=0 \tag{11}$$

where $Sc=\frac{\upsilon}{D_M}$ is the Schmidt number, $K=\frac{\kappa}{\mu}$ is the material parameter, $Pr=\frac{\rho\upsilon C_P}{k}$ is the Prandtl number, $Ec=\frac{u_w^2}{C_P(T_w-T_\infty)}$ is the Eckert number, $K_C=\frac{k_0}{b}$ is the chemical reaction parameter, $M=\frac{\pi j_0 M_0}{8\rho x b^2}$ is the modified Hartmann number, $\beta=\frac{\pi}{d}\sqrt{\frac{\upsilon}{b}}$ is width variable, $Du=\frac{D_M K_T(C_w-C_\infty)}{\upsilon C_S C_P(T_w-T_\infty)}$ is Dufour (thermo-diffusion) parameter, $Sr=\frac{D_M K_T(T_w-T_\infty)}{\upsilon T_M(C_w-C_\infty)}$ is Soret (diffusion-thermo) parameter.

The corresponding boundary conditions are:

$$\left.\begin{array}{l}\text{At } \eta=0:\ f'=1,\ f=0,\ g=0,\ \theta=1,\ \phi=1\\ \text{As } \eta\to\infty:\ f'=0,\ g=0,\ \theta=0,\ \phi=0\end{array}\right\} \tag{12}$$

Physical quantities of interest

The quantities of physical interest are the skin-friction coefficient, the local heat transfer (Nusselt number) and the local mass transfer (Sherwood number).

The wall shear stress is given by

$$\tau_w=\left[(\mu+\kappa)\frac{\partial u}{\partial y}+\kappa N\right]_{y=0}=bx(\mu+\kappa)\sqrt{\frac{b}{\upsilon}}f''(0) \tag{13}$$

The local skin friction coefficient (C_f) is defined as:

$$C_f = \frac{\tau_w}{\rho u_w^2} = \frac{1+K}{\sqrt{\mathrm{Re}_w}} f''(0) \tag{14}$$

The rate of heat transfer from the wall q_w is

$$q_w = -k\left(\frac{\partial T}{\partial y}\right)_{y=0} = -k\left(T_w - T_\infty\right)\sqrt{\frac{b}{\upsilon}}\,\theta'(0) \tag{15}$$

The Nusselt number Nu is given by

$Nu = \dfrac{xq_w}{k\left(T_w - T_\infty\right)}$. Using equation (15), we get $\dfrac{Nu}{\sqrt{Re_w}} = -\theta'(0)$ (16)

The equation defining the couple's stress is

$$M_w = j\left(\mu + \frac{\kappa}{2}\right)\left(\frac{\partial N}{\partial y}\right)_{y=0} \tag{17}$$

Consequently, the dimensionless couple stress is given by

$$M_x = -\frac{M_w}{\mu u_w} = -\frac{1}{j}\left(1+\frac{K}{2}\right)g'(0) \tag{18}$$

The mass flux can be defined as

$$j_w = -D_M\left(\frac{\partial C}{\partial y}\right)_{y=0} = -D_M\left(C_w - C_\infty\right)\sqrt{\frac{b}{\upsilon}}\,\phi'(0) \tag{19}$$

Sherwood number Sh is defined as

$Sh = \dfrac{j_w x}{D_M\left(C_w - C_\infty\right)}$ where $Re_w = \dfrac{bx^2}{\upsilon}$ is the local Reynolds number. (20)

3. Methodology

We have solved the non-linear differential equations (8)-(11) along with the boundary conditions (12) numerically by developing programming codes in MATLAB using the shooting method along with the fourth order Runge-Kutta scheme. The coupled nonlinear ordinary differential equations, along with the

boundary conditions, have been transformed into a system of simultaneous first--order equations for the unknowns using the method of superposition. To proceed, we define the following:

$$y_1 = f,\ y_2 = f',\ y_3 = f'',\ y_4 = g,\ y_5 = g',\ y_6 = \theta,\ y_7 = \theta',\ y_8 = \phi,\ y_9 = \phi'.$$

Using these, equations (8)-(11) can be written as

$$y_3' = \frac{1}{(1+K)}\left[-y_1 y_3 - K y_5 - M e^{-\beta\eta} + (y_2)^2\right] \tag{21}$$

$$y_5' = \frac{1}{\left(1+\frac{K}{2}\right)}\left[-y_1 y_5 + y_2 y_4 + K(2y_4 + y_3)\right] \tag{22}$$

$$y_7' = \frac{1}{(1-\mathrm{PrDuScSr})}\left[-\mathrm{Pr}\, y_1 y_7 - (1+K)\,\mathrm{PrEc}(y_3)^2 - \mathrm{PrDuSc}\, y_1 y_9 - \mathrm{PrDuScKc}\, y_8\right] \tag{23}$$

$$y_9' = \frac{1}{(1-\mathrm{PrDuScSr})}\left[-\mathrm{Sc}\, y_1 y_9 + \mathrm{ScKc}\, y_8 + \mathrm{ScSrPr}\, y_1 y_7 + (1+K)\,\mathrm{SrScPrEc}(y_3)^2\right] \tag{24}$$

With the boundary condition

$$\left.\begin{aligned} &y_1(0) = 0,\ y_2(0) = 1,\ y_4(0) = 0,\ y_6(0) = 1,\ y_8(0) = 1 \\ &y_2(\infty) = 0,\ y_4(\infty) = 0,\ y_6(\infty) = 0,\ y_8(\infty) = 0 \end{aligned}\right\} \tag{25}$$

To integrate equations (21)-(24), appropriate initial guess values for the missing boundary conditions are selected, followed by the integration process.

4. Results and discussion

The nonlinear governing equations (8) to (11) with boundary conditions (12) have been solved numerically using the shooting method with the Runge-Kutta scheme. It is seen that the convergence of the iteration process is quite rapid.

From Figures 3-18, we have shown the effect of physical quantities such as *M*, *K*, *Pr*, *Ec*, *Sc*, *Sr* and *Du* on fluid velocity, angular velocity, fluid temperature and fluid concentration.

Figures 3 and 4 illustrate the impact of Hartman number (*M*) and material parameter (*K*) on the velocity profile. From Figure 3, it is observed that flow velocity increases with the increasing values of *M*. Due to the dominant influence of the

induced Lorentz force in the positive x-direction, higher values of the modified Hartman number indicate an increasing trend. Figure 4 shows that the velocity profile increases with the increasing values of K. With an increase in K, the micro-concentration of the fluid also increases, leading to changes in the flow behavior. Consequently, the boundary layer thickness increases.

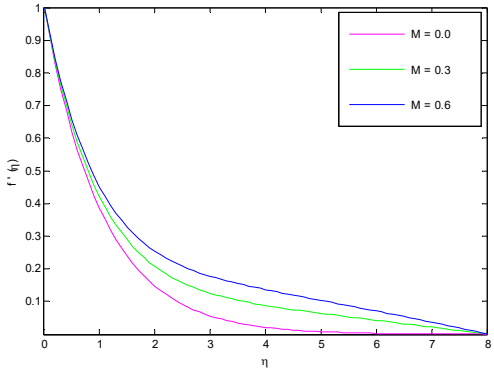

Fig. 3. Velocity profile for different values of M

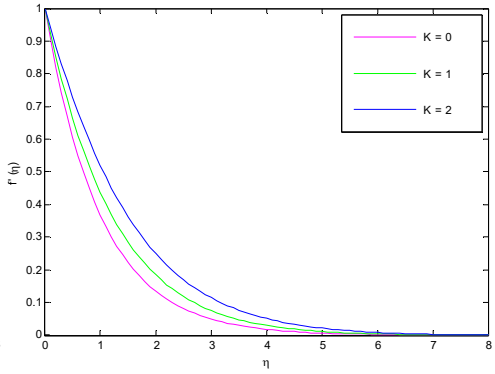

Fig. 4. Velocity profile for different values of K

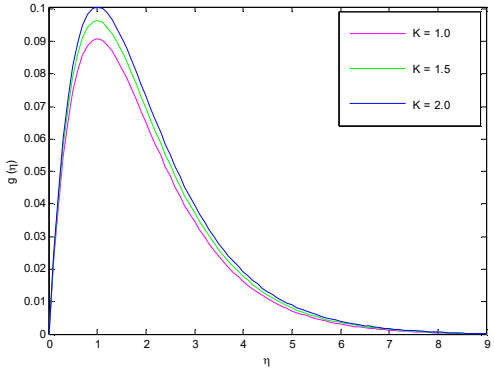

Fig. 5. Angular velocity profile for different K

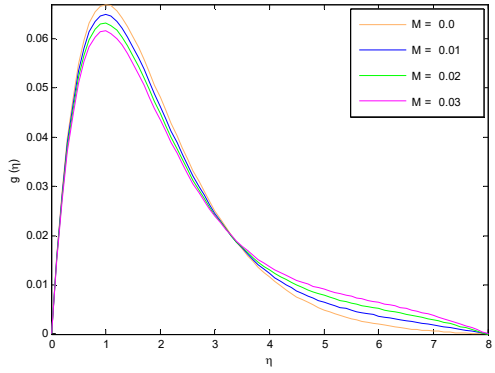

Fig. 6. Angular velocity profile for different M

Figures 5 and 6 demonstrate the effect of K and M on the angular velocity profile. Figure 5 reveals that the angular velocity increases significantly for larger values of the material parameter K. Figure 6 depicts that angular velocity decreases until it reaches the position $\eta \leq 3.4$ and, thereafter, a reversed effect is observed.

Figure 7 is plotted to understand how the magnetic parameter M influences the temperature profile. It is seen that the temperature profile decreases with M. Figure 8 indicates how temperature profile changes with K. It is observed that the temperature profile declines with K. The effect of Pr on the temperature profile is shown in Figure 9. It is seen that temperature profile decreases with Pr. This is due to the fact that, when the Pr increases, the thermal conduction of the medium decreases, leading to a reduction in the thermal boundary layer thickness.

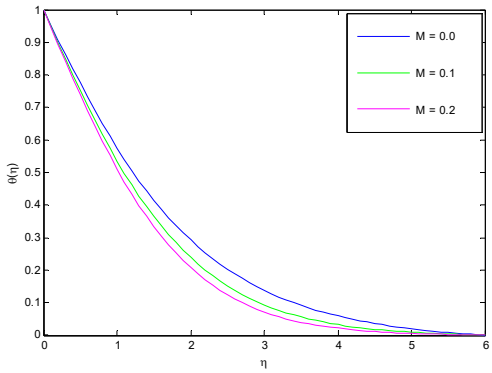

Fig. 7. Temperature profile for variation of *M*

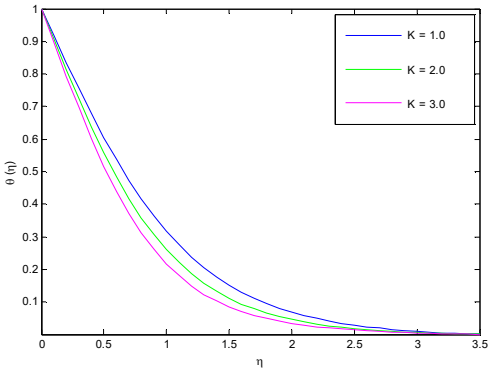

Fig. 8. Temperature profile for variation of *K*

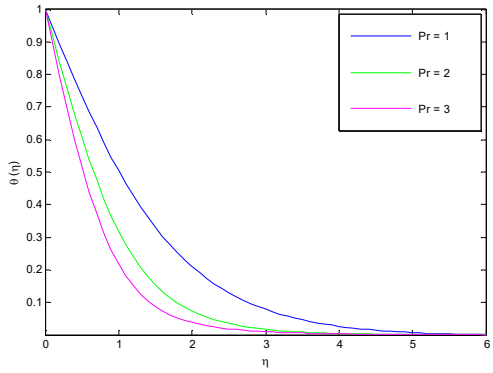

Fig. 9. Temperature profile for variation of *Pr*

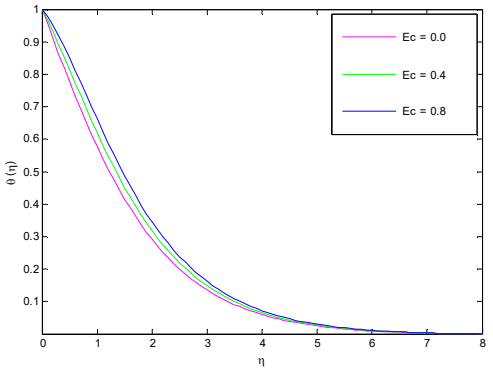

Fig. 10. Temperature profile for variation of *Ec*

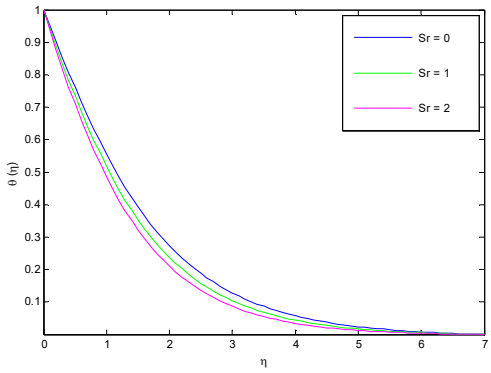

Fig. 11. Temperature profile for variation of *Sr*

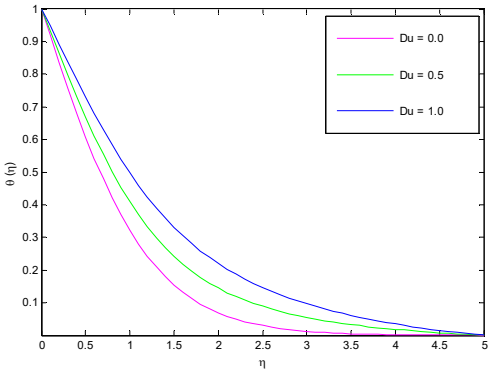

Fig. 12. Temperature profile for variation of *Du*

The effect of *Ec* on the temperature profile is given in Figure 10. It has been found that increasing the value of *Ec* causes enhancement in temperature distribution and boundary layer thickness. Figure 11 shows the effect of *Sr* on the temperature profile, and it is observed that the temperature profile decreases with *Sr*.

An increase in *Sr* leads to a decrease in the thermal boundary layer thickness, resulting in a reduction in temperature. Figure 12 depicts the impact of *Du* on temperature profile. It is evident that temperature profile increases with *Du*.

Figure 13 depicts the impact of *M* on the concentration profile. It is seen that the temperature profile decreases with *M*. Figure 14 highlights the effect of *K* on the concentration profile. This shows that concentration profile decreases with the increasing values of *K*.

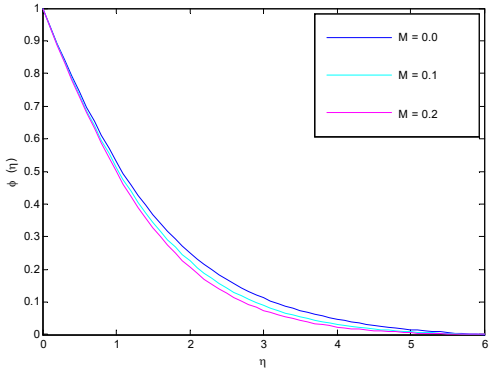

Fig. 13. Concentration profile for variation of *M*

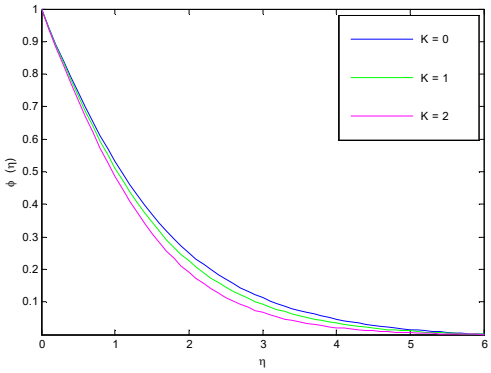

Fig. 14. Concentration profile for variation of *K*

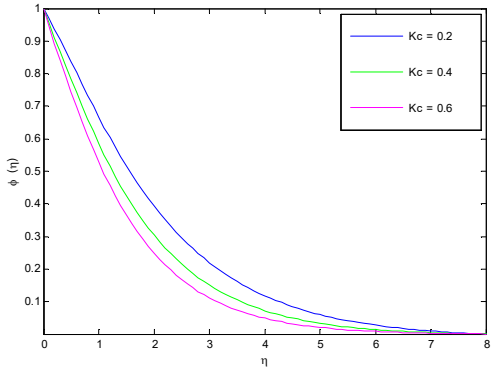

Fig. 15. Concentration profile for variation of *Kc*

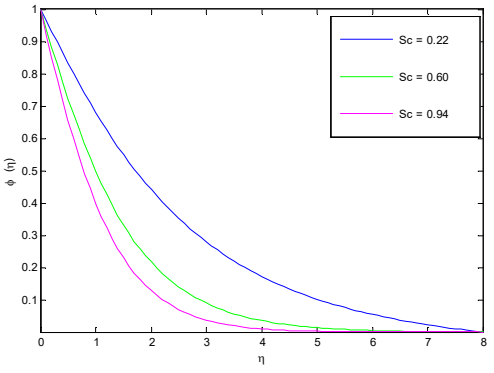

Fig. 16. Concentration profile for variation of *Sc*

Figure 15 illustrates the variation of concentration profiles with *Kc*. It is found that the concentration profile decreases with *Kc*. This is because the chemical reaction in this system consumes the chemical, resulting in a reduction in the concentration profile. Figure 16 shows the effect of *Sc* on the concentration profile, It is observed that the concentration profile decrease with *Sc*. An increase in *Sc* results in a reduction in the molecular or mass diffusivity of the fluid, leading to a decrease in the concentration of fluid particles. Figure 17 and 18 illustrate the impact of *Sr* and *Du* on concentration profile. From Figure 17, it is observed that fluid concentration increases with *Sr*. Elevated values of *Sr* lead to a stronger convective

flow, resulting in an increase in concentration. From Figure 18, it is seen that there is a decrease in fluid concentration until it reaches $\eta \leq 1.4$ and thereafter the reverse effect is observed.

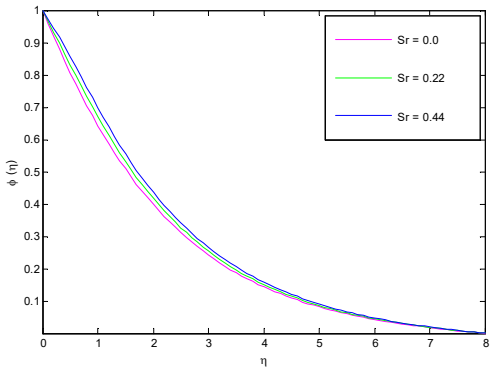

Fig. 17. Concentration profile for variation of *Sr*

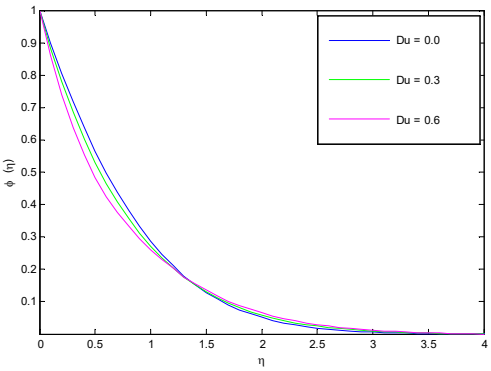

Fig. 18. Concentration profile for variation of *Du*

Table 1 illustrates the changes in $-f''(0)$, $-\theta'(0)$ and $-\phi'(0)$ due to the influence of M, K, and β, which shows a good agreement with the previously published work by Reddy et al. [21].

Table 1. Comparison results for $-f''(0)$, $-\theta'(0)$ and $-\phi'(0)$ for different values of M, K and β at $Pr = 6.2$, $Sc = 0.22$, $Ec = 0.02$ and $Kc = 0.1$

M	K	β	$-f''(0)$		$-\theta'(0)$		$-\phi'(0)$	
			Reddy et al. [21]	Present study	Reddy et al. [21]	Present study	Reddy et al. [21]	Present study
0	0.2	1	0.90975	0.909747	1.865537	1.865467	0.26522	0.26531
0.5			0.699167	0.699163	1.900295	1.900268	0.280001	0.280001
1			0.496288	0.496281	1.930793	1.930774	0.292783	0.292773
1	0	1	0.950328	0.950329	1.84571	1.84569	0.262482	0.262457
	0.5		0.769444	0.769439	1.906578	1.906561	0.27529	0.27533
	2		0.520359	0.520352	2.017546	2.017552	0.296674	0.296665
1	0.2	0.2	0.815108	0.815102	1.883016	1.883025	0.285358	0.285345
		0.4	0.837795	0.837789	1.878961	1.878954	0.276605	0.276619
		0.6	0.851606	0.851611	1.876191	1.876189	0.272101	0.272096

From Table 2, it has been observed that the skin friction coefficient represented by C_f decreases with increasing values of Hartman number (M) whereas, an opposite effect has been observed for the rate of local heat transfer in terms of Nusselt number (Nu) and the rate of mass transfer in terms of Sherwood number (Sh).

With the increase of *Sr*, Nusselt number (*Nu*) increases but the Sherwood number (*Sh*) decreases. In case of Dufour number (*Du*), opposite results are seen i.e., *Nu* decreases and *Sh* increases with the increasing values of *Du*.

Table 2. Values of skin friction coefficient (C_f), Nusselt number (*Nu*) and Sherwood number (*Sh*) for various values of *M*, *Sr*, and *Du*

M	*Sr*	*Du*	C_f	*Nu*	*Sh*
0.1	0.1	0.3	0.43329	3.616441	0.868689
0.2			0.37625	3.707640	0.889100
0.3			0.32444	3.778522	0.905946
0.4	0.4	0.41	0.23024	1.191935	0.927263
	0.5		0.23024	1.194861	0.912911
	0.6		0.23024	1.197814	0.898445
0.5	0.7	0.7	0.19107	1.145721	0.906952
		0.8	0.19107	1.113047	0.911030
		0.9	0.19107	1.079863	0.915179

5. Conclusion

In the present study, the heat and mass transport phenomena of MHD micropolar fluid flow over a vertically stretched Riga plate with the Soret and Dufour effect are examined numerically. The collective impact of the Soret effect, Dufour effect, micropolar, magnetic field and chemical reaction over a Riga plate are described. The results of this study provide a flow and heat transfer analysis in a micropolar fluid, which will aid other investigators or engineers in selecting suitable parameters for heat transfer optimisation in modern industry. From this present investigation, it can be concluded that:

- The velocity of the fluid increase by increasing the value of Hartman number (*M*) and material parameter (*K*).
- Higher values of material parameter *K*, angular velocity or micro-rotation $g(\eta)$ is higher while the effect of magnetic field is almost opposite.
- The temperature distribution $\theta(\eta)$ decreases with *M*, *K*, *Pr* and *Sr*, whereas increases with *Ec* and *Du*.
- As the Hartman number and material parameter increased, concentration $\phi(\eta)$ decreases.
- An increase of the Soret number (*Sr*) leads to an increase of the concentration profile.
- The magnitude of the skin friction coefficient is less significant for micropolar fluids.
- This analysis has revealed that the flow field has a significant effect on the Magnetic parameter (*M*), Soret numbers (*Sr*), and Dufour numbers (*Du*).

Nomenclature

u, v Velocity components along x and y direction [m s^{-1}]
μ Coefficient of dynamic viscosity [kg m^2 s^{-1}]
ρ Free stream density [kg m^{-3}]
υ Coefficient of kinematic viscosity [m^2 s^{-1}]
d Width of magnets and electrodes
κ Coefficient of Vortex viscosity
N Angular velocity or micro-rotation
γ Viscosity of spin gradient
b Constant
k Thermal conductivity [ω m^{-1} K^{-1}]
β Dimensionless parameter
D_M Chemical molecular diffusivity [m^2 s^{-1}]
j_0 Current Density
j Micro inertia density
M_0 Magnetization of permanent magnet
C_P Specific heat at constant pressure [J kg^{-1} K^{-1}]
u_w Surface velocity [m s^{-1}]
C Concentricity [mol m^{-3}]
C_w Species concentration at the surface [mol m^{-3}]
C_∞ Fluid concentration outlying the surface [mol m^{-3}]
T Temperature [K]
T_w Wall temperature [K]
T_∞ Ambient temperature [K]
Pr Prandtl number
Ec Eckert number
K_C Chemical reaction parameter
Du Dufour Number
K Material parameter
ψ Stream function [m^2 s^{-1}]
θ Dimensionless temperature [K]
ϕ Dimensionless concentration [mol m^{-3}]
C_f The local skin friction coefficient
Nu Nusselt number
S_h Sherwood number
Sc Schmidt number
M Modified Hartman number
Sr Soret Number
τ_w Wall shear stress

References

[1] Eringen, A. (1964). Simple microfluids. *International Journal of Engineering Science*, *2*(2), 205-217.

[2] Eringen, A. (1966). Theory of micropolar fluids. *Journal of Mathematics and Mechanics*, *16*(1), 1-18.

[3] Hassanien, I.A., & Gorla, R.S.R. (1990). Heat transfer to a micropolar fluid from a non-isothermal stretching sheet with suction and blowing. *Acta Mechanica*, *84*, 191-199.

[4] Gailitis, A., & Lielausis, O. (1961). On a possibility to reduce the hydrodynamic resistance of a plate in aelectro-lyte. *Applied Magnetohydrodynamics*, *13*, 143-146.

[5] Ahmad, R., Mustafa, M., & Turkyilmazoglu, M. (2007). Buoyancy effects on nanofluid flow past a convectively heated vertical Riga-plate: A numerical study. *International Journal of Heat and Mass Transfer*, *111*, 827-835.

[6] Ayub, M., Abbas, T., & Bhatti, M.M. (2016). Inspiration of slip effects on electromagnetohydro-dynamics (EMHD) nanofluid flow through a horizontal Riga plate. *The European Physical Journal Plus*, *131*, 1-9.

[7] Hayat, T., Abbas, T., Ayub, M., Farooq, M., & Alsaedi A. (2016). Flow of nanofluid due to convectively heated Riga plate with variable thickness. *Journal of Molecular Liquids*, *222*, 854-862.

[8] Iqbal, Z., Azhar, E., Mehmood, Z., & Maraj, E. (2017). Melting heat transport of nanofluidic problem over a Riga plate with erratic thickness: Use of Keller Box scheme. *Results in Physics*, *7*, 3648-3658.

[9] Rasool, G., & Zhang, T. (2019). Characteristics of chemical reaction and convective boundary conditions in Powell-Eyring nanofluid flow along a radiative Riga plate. *Heliyon*, *5*(4), e01479.

[10] Fatunmbi, E.O., & Adeosun, A.T. (2020). Nonlinear radiative Eyring-Powell nanofluid flow along a vertical Riga plate with exponential varying viscosity and chemical reaction. *International Communications in Heat and Mass Transfer*, *119* (104913).

[11] Reddy, G.V.R., & Krishna, Y.H. (2018). Soret and Dufour effects on MHD micropolar fluid flow over a linearly stretching sheet, through a non-darcy porous medium. *International Journal of Applied Mechanics and Engineering*, *23*(2), 485-502.

[12] Reddy, Y.D., Goud, B.S., Nalivela, N.R., & Rao, V.S. (2023). Impact of porosity on two-dimensional unsteady MHD boundary layer heat and mass transfer stagnation point flow with radiation and viscous dissipation. *Numerical Heat Transfer, Part A: Applications*. DOI: 10.1080/10407782.2023.2198739.

[13] Goud, B.S., Reddy, Y.D., & Asogwa K.K. (2023). Chemical reaction, Soret and Dufour impacts on magnetohydrodynamic heat transfer Casson fluid over an exponentially permeable stretching surface with slip effects, *International Journal of Modern Physics B*, *37*(13), 2350124. DOI: 10.1142/S0217979223501242.

[14] Mishra, P., Kumar, D., Reddy, Y.D., & Goud, B.S. (2022). Numerical investigation of MHD flow of Williamson nanofluid with variable viscosity pasting a wedge within porous media: A non-Darcy model approach. *Heat Transfer*, *51*(7), 6071-6086. DOI: 10.1002/htj.22580.

[15] Goud, B.S., & Reddy Y.D. (2022). Chemical reaction and Soret effect on an unsteady MHD heat and mass transfer fluid flow along an infinite vertical plate with radiation and heat absorption. *Journal of the Indian Chemical Society*, *99*(11), 100762. DOI: 10.1016/j.jics.2022.100762.

[16] Reddy, Y.D., Goud, B.S., Nisar, K.S., Alshahrani, B., Mahmoud, M., & Park, C. (2023). Heat absorption/generation effect on MHD heat transfer fluid flow along a stretching cylinder with a porous medium. *Alexandria Engineering Journal*, *64*, 659-666. DOI: 10.1016/j.aej.2022.08.049.

[17] Goud, B.S., Reddy, Y.D., & Asogwa, K.K. (2022). Inspection of chemical reaction and viscous dissipation on MHD convection flow over an infinite vertical plate entrenched in porous medium with Soret effect. *Biomass Conversion and Biorefinery*. DOI: 10.1007/s13399-022-02886-3.

[18] Kumar, M.A., Reddy, Y.D., Goud, B.S., & Rao, V.S. (2022). An impact on Non-Newtonian free convective MHD Casson fluid flow past a vertical porous plate in the existence of Soret, Dufour, and chemical reaction. *International Journal of Ambient Energy*, *43*, 1-26. DOI: 10.1080/01430750.2022.2063381.

[19] Reddy, N.N., Reddy, Y.D., Rao, V.S., Goud, B.S., & Nisar, K.S. (2022). Multiple slip effects on steady MHD flow past a non-isothermal stretching surface in presence of Soret, Dufour with suction/injection. *International Communications in Heat and Mass Transfer*, *134*, 106024. DOI: 10.1016/j.icheatmasstransfer.2022.106024.

[20] Ahmed, B., Akbar, F., Ghaffari, A., Khan, S.U., Khan, M.I., & Reddy, Y.D. (2022) Soret and Dufour aspects of the third-grade fluid due to the stretching cylinder with the Keller box approach. *Waves in Random and Complex Media*. DOI: 10.1080/17455030.2022.2085891.

[21] Goud, B.S., Reddy, Y.D., Alshehri, N.A., Jamshed, W., Safdar, R., Eid, M.R., & Bouazizi, M.L. (2022). Numerical case study of chemical reaction impact on MHD micropolar fluid flow past over a vertical Riga plate. *MDPI-Materials*, *15* (4060).